Article

Heuristic Approaches Based on Modified Three-Parameter Model for Inverse Acoustic Characterisation of Sintered Metal Fibre Materials

Tianfei Zhao [1,†], Baorui Pan [1,†] , Xiang Song [1], Dan Sui [1], Heye Xiao [2] and Jie Zhou [1,*]

1 School of Aeronautics, Northwestern Polytechnical University, Xi'an 710072, China
2 Unmanned System Research Institute, Northwestern Polytechnical University, Xi'an 710072, China
* Correspondence: jiezhou@nwpu.edu.cn
† These authors contributed equally to this work.

Abstract: Modelling of sound propagation in porous media generally requires the knowledge of several transport properties of the materials. In this study, a three-parameter analytical model that links microstructure properties of sintered metal fibre materials and non-acoustical parameters of the JCAL model is used and modified, and two heuristic approaches based on the established model for inverse acoustic characterisation of fibrous metal felts are developed. The geometric microstructure of sintered fibrous metals is simplified to derive the relationship between pores and fibre diameters. The new set of transport parameters in the modified three-parameter model can cover two controllable parameters during the fabrication process of fibrous metals. With two known transport parameters, six sintered specimens are characterised using a deterministic algorithm, and a satisfactory result is achieved in fitting the normalised surface impedance measured by an acoustic measurement system. Moreover, the forward evaluation shows that our modified three-parameter theoretical model is capable of yielding accurate results for the sintered metal fibre materials. A numerical investigation of the complete inverse acoustic characterisation of fibrous metals by a global non-deterministic algorithm indicates that inversion from two porous material properties is preferable to the normalised surface impedance.

Keywords: sintered metal fibre materials; inverse problem; heuristic optimisation; microstructure-based acoustic model

MSC: 74J05

1. Introduction

Sintered metal fibre felts, typically fabricated using micron-sized FeCrAl fibres, are a new engineering material. Compared with conventional fibrous materials, e.g., glass fibre and polyester, sintered metal fibre materials possess not only excellent sound absorption ability, but also exhibit many functional properties: good mechanical properties, high thermal stability, easy processability, and long-life, etc. [1–3]. Therefore, sintered metal fibre materials are particularly suitable for applying noise reduction and vibration control under extreme conditions, such as high pressure and temperature [4].

In order to give a physical basis to the description of the macroscopic acoustic behaviour of porous media, a variety of semi-phenomenological models involving several physical parameters have been presented, such as the Delany–Bazley–Miki model (one parameter) [5,6], the Johnson–Champoux–Allard (JCA) model (five parameters) [7–9], the Johnson–Champoux–Allard–Lafarge (JCAL) model (six parameters) [7,8,10], the Johnson–Champoux–Allard–Pride–Lafarge (JCAPL) model (eight parameters) [7,8,10,11] and the Biot's theory [12,13]. Apart from the direct use of these models to predict sound propagation in porous media [14–20], the inverse acoustic characterisation from the acoustical properties of materials is also of great interest for its practical values in engineering application [21],

e.g., inverse design of fibrous metals for achieving high absorption at desired frequencies. Hence, the modelling of sound propagation in sintered metal fibre materials requires the known set of several transport properties, such as porosity, permeability, and characteristic length [22]. To estimate these properties, many methods for characterisation of porous media have been developed, three main of which include: direct, indirect, and inverse methods. Direct methods are based on various experiments, which can directly obtain a set of properties, e.g., porosity, static air flow resistivity, tortuosity, two characteristic lengths, and two permeabilities [23–26]. Such approaches provide the most accurate and reliable measured parameters among the three methods while suffering the disadvantage of the huge cost and the complex experiment procedures. For indirect methods, based on equivalent fluid models assume, the equivalent density and equivalent bulk modulus of porous media obtained from several different methods of impedance tube measurement are used to analyse the transport properties of porous materials [27–30].

As an alternative solution to another two methods for obtaining the physical parameters from materials, inverse methods transform the physical problem into a mathematical optimisation problem, which directly estimates transport parameters from acoustical properties measured by impedance tube. Previous existing studies on the inverse characterisation of porous media can be divided into two categories: deterministic or non-deterministic parametric inversion methods and statistical inversion methods. The first relies on local or global optimisation algorithms in fitting the curves of acoustical properties from impedance tube or ultrasonic measurements Atalla and Panneton [31] proposed an inverse characterisation method based on normalised surface impedance and yielded three of five JCA transport parameters by using a differential evolution algorithm Dauchez and Yvars [32] employed the constraint satisfaction problem approach to an inverse procedure for recovering all five parameters of the JCA model from the density and bulk modulus of the equivalent fluid. Furthermore, Dossi et al. [33] proposed an inverse calculation of the elastic parameters of polyurethane foams by fitting measured specific acoustic impedance from samples with different thicknesses. The statistical inversion methods, capable of taking into account knowledge of uncertainty of measurement process and prior information, have been developed to estimate uncertainty for the pore parameter values Chazot et al. [34] introduced a Bayesian approach for evaluating eight properties of Biot's model with a measurement in a standing wave tube and returning probabilistic data such as the confidence interval of all parameters Niskanen et al. [35] and Cuenca et al. [36] proposed a deterministic and statistical framework for inverse characterisation, in which the minimum obtained by the least-squares method was validated using the information given by the statistical inversion and uncertainties in the estimations could be quantified.

Most existing works on the inverse calculation of transport parameters employed the JCA/JCAL or Biot-JCA model [12,13]. The first two are based on equivalent fluid models assume, while the latter one considers the solid phase of porous media as an elastic material. For sintered metal fibre felts, the frame of this material can be assumed motionless in all frequency ranges due to its quite low decoupling frequency and barely visible resonance behaviour. Thus, the equivalent fluid description for fibrous metals is employed in this study. Some researchers suggested that the classical parametrisation of the acoustical behaviour of certain types of porous media is somewhat redundant [36,37]. Additionally, all the above-mentioned methods can suffer from the accuracy of the experiment and the ill condition of the inverse problem, respectively.

For that purpose, in this study, we develop two heuristic approaches using a modified three-parameter analytical model to investigate the inverse acoustic characterisation of sintered metal fibre materials. First, the three-parameter analytical model for the non-acoustical properties based on the JCAL model is provided and modified based on the average pore size approximation according to the microstructure characteristics of the fibrous metals. Then, the normalised surface impedance of six samples is measured by a classic two-microphone impedance tube measurement. The proposed modified model is validated through the curve fitting with a single parameter estimation of measured data using a local optimisation algorithm. The theoretical model established is employed

to examine the difference between the values recovered from surface impedance and those from two porous material properties with a global optimisation algorithm in the numerical investigation.

This paper is organised as follows. First, Section 2 presents the three-parameter analytical model and derives the geometric relationship between pores and fibre diameters according to the simplified microstructure of sintered fibrous metals. The measurement set-up based on a two-microphone configuration is outlined in Section 3. Section 4 describes the observation model of measurements along with the two representative heuristic approaches. Next, Section 5 presents the verification of the theoretical model and numerical investigation with two heuristic methods. Section 6 concludes this study and discusses related future work aspects.

2. Acoustic Modelling of the Sintered Fibrous Metals

2.1. Three-Parameter Analytical Model

The well-established Johnson–Champoux–Allard–Lafarge (JCAL) model for sound propagation in porous media proposed by Champoux, Allard, and Lafarge relies on six transport parameters: porosity ϕ, flow resistivity σ, tortuosity α_∞, viscous characteristic length Λ, thermal characteristic length Λ' and static thermal permeability k'_0. It has been shown that the popular six-parameter model can be simplified, and the use of three parameters in the JCAL model is enough for some types of porous media. In our study, a three-parameter analytical model based on the JCAL model proposed by Horoshenkov et al. [37] is adopted. The choice of using this model instead of others is motivated by the following three reasons:

1. This theoretical model links three pore parameters of porous media to six non-acoustical parameters in the JCAL model, which lay the groundwork for the study of using customisable morphological parameters of real fibrous metals replacement to the transport parameters that are difficult to measure;
2. The JCAL model, which introduces corrections to the bulk modulus thermal behaviour at low frequencies that is not captured by the JCA model, its robustness has been validated by many studies.
3. Halving the number of variables can significantly reduce the complexity of the inverse characterisation problem, thus reducing uncertainty and consumption of time in computation during the inversion procedure.

As previously discussed, with the skeleton of sintered metal fibre materials being far heavier than air, the frame can be almost motionless for large ranges of acoustical frequencies. In other words, fibrous metals can be assumed as an equivalent fluid with an equivalent effective density $\rho_{eq}(\omega)$ and equivalent bulk modulus $K_{eq}(\omega)$ used to describe the macroscopic acoustical behaviour of the material. Based on the six transport parameters presented previously, the expressions of $\rho_{eq}(\omega)$ and K_{eq} used for the JCAL model are given by [7,8,10]:

$$\rho_{eq}(\omega) = \frac{\alpha_\infty \rho_0}{\phi} \left[1 + \frac{\sigma \phi}{j\omega \rho_0 \alpha_\infty} \sqrt{1 + j\frac{4\alpha_\infty^2 \eta \rho_0 \omega}{\sigma^2 \Lambda^2 \phi^2}} \right] \tag{1}$$

$$K_{eq}(\omega) = \frac{\gamma P_0 / \phi}{\gamma - (\gamma - 1)\left[1 - j\frac{\phi \kappa}{k'_0 C_p \rho_0 \omega}\sqrt{1 + j\frac{4k_0'^2 C_p \rho_0 \omega}{\kappa \Lambda'^2 \phi^2}}\right]^{-1}} \tag{2}$$

where $j = \sqrt{-1}$, ρ_0 is the density of air, α_∞ is the tortuosity, ϕ is the porosity, σ is the flow resistivity, η is the dynamic viscosity of the fluid, γ is the specific heat ratio, k'_0 is the static thermal permeability, Λ is the viscous characteristic length, Λ' is the thermal characteristic length, P_0 is the quiescent pressure, κ is the thermal conductivity, C_p is the specific heat.

The shape of pores in the majority of realistic porous materials is variable, and the size normally obeys a particular statistical distribution. For sintered metal fibre material, based on the prior assumptions of log-normal distribution of pore size, the five of six transport

parameters in Equations (1) and (2) can be expressed via three pore parameters using the three-parameter model: the porosity ϕ, average pore size $\bar{s}$ and standard deviation in the pore size σ_s, which are given, respectively, as follows [37]:

$$\Lambda = \bar{s}e^{-5/2(\sigma_s \log 2)^2}, \tag{3}$$

$$\Lambda' = \bar{s}e^{3/2(\sigma_s \log 2)^2}, \tag{4}$$

$$k_0' = \frac{\bar{s}^2 \phi}{8\alpha_\infty}e^{6(\sigma_s \log 2)^2}, \tag{5}$$

$$\alpha_\infty = e^{4(\sigma_s \log 2)^2}, \tag{6}$$

$$\sigma = \frac{8\eta\alpha_\infty}{\bar{s}^2 \phi}e^{6(\sigma_s \log 2)^2}. \tag{7}$$

Under the assumption of an equivalent fluid model, the specific characteristic impedance Z_c and the complex wave number k_c of fibrous metal materials can be calculated as [22]:

$$Z_c = \frac{\sqrt{\rho_{eq}(w)K_{eq}(w)}}{\rho_0 c_0}, \tag{8}$$

$$k_c = w\sqrt{\frac{\rho_{eq}(w)}{K_{eq}(w)}}. \tag{9}$$

where c_0 is the sound velocity in the air.

2.2. Average Pore Size Approximation

As a kind of fibrous material, the commonly used non-acoustical parameters to characterise the sintered metal fibre felts are porosity ϕ and fibre diameter d. These two parameters can be precisely controlled during the fabrication process of fibrous metals. This section aims to link porosity ϕ and fibre diameter d to the average pore size $\bar{s}$ that is not a controllable parameter during the manufacturing process. The purpose is to obtain the quantitative relation among three geometrical parameters.

The 3D digital model of a fibrous metal felt reconstructed by Micro-computed tomography (micro-CT) [38] is displayed in Figure 1. As shown in Figure 1a, the composition of the real fibrous metals is twisted metal fibres which are connected by the sintered points after the sintering process. The front view of the slice image in the red square plane is illustrated in Figure 1a is provided in Figure 2a. A thin slice thickness along the x axis is made, thus, the fibre orientation can be observed intuitively in this 3D slice image. Fibres are randomly positioned and horizontal obliquely to the image plane. Combined with Figures 1b,c and 2a, it can be seen that the intersecting fibres lie in the x-y plane parallel to the surface of fibrous metal felts. In order to build relations between geometrical parameters, a cell method proposed by Tarnow [39,40] is used. A Voronoi-based segmentation is performed on the 2D slice image after the binary process, as shown in Figure 2b. Each oval fibre cross-section is surrounded by a so-called Voronoi polygon. It is constructed by drawing perpendicular bisectors passing through the midpoints between each centre and the nearest neighbour centres. These lines intersect and form the Voronoi polygons. The distance between one centre and the nearest neighbour centre can be regarded as the pore size. It has been demonstrated that any Voronoi polygon is necessarily convex. Since sound normally incidents on the surface of felts, we consider a simplified model that the fibres are all parallel and regularly placed and in the same diameter, as shown schematically in Figure 2c, the sound wave incident perpendicularly passes all cylindrical fibres, i.e., parallel to the z axis. In this case, the irregular Voronoi polygons displayed in Figure 2b can

be approximated to regular hexagons. The distance between the centre of one cylindrical fibre and any nearest neighbour fibre is equal to the average pore size $\bar{s}$. For simplicity, each ideal hexagonal Voronoi region is approximated by an inscribed circle having the approximate area. The porosity of one unit cell in the parallel cylindrical fibres array is identical to that of the macroscopical homogeneous sintered metal fibrous material. Then the equivalent porosity of the randomly distributed fibres can be given by

$$\phi = \frac{\pi(\bar{s}/2)^2 - \pi(d/2)^2}{\pi(\bar{s}/2)^2}, \tag{10}$$

where the porosity ϕ and the fibre diameter d are assumed known, thus the average pore size $\bar{s}$ can be eventually represented as

$$\bar{s} = \frac{d}{\sqrt{1-\phi}}. \tag{11}$$

By substituting Equation (11) into Equations (3)–(7), the transport parameters of the JCAL model can be calculated by a new set of parameters in modified three-parameter model, i.e., the porosity ϕ, fibre diameter d and standard deviation in the pore size σ_s, as follows:

$$\Lambda = \frac{d e^{-5/2(\sigma_s \log 2)^2}}{\sqrt{1-\phi}}, \tag{12}$$

$$\Lambda' = \frac{d e^{3/2(\sigma_s \log 2)^2}}{\sqrt{1-\phi}}, \tag{13}$$

$$k_0' = \frac{d^2\phi}{8\alpha_\infty(1-\phi)} e^{6(\sigma_s \log 2)^2}, \tag{14}$$

$$\alpha_\infty = e^{4(\sigma_s \log 2)^2}, \tag{15}$$

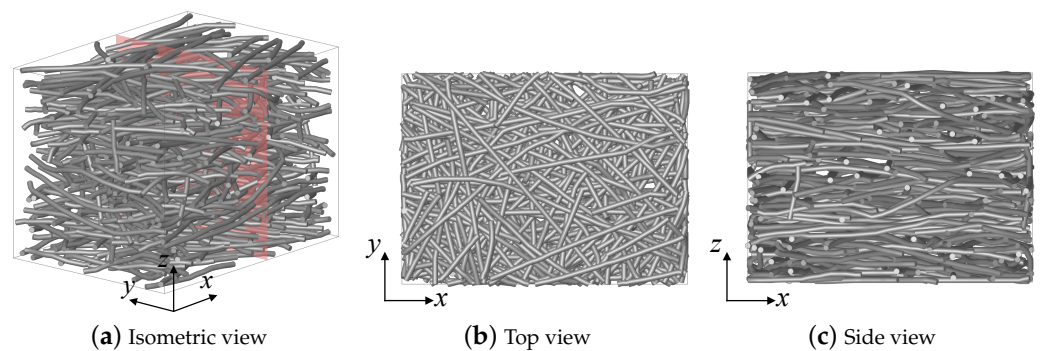$$\sigma = \frac{8\eta\alpha_\infty(1-\phi)}{d^2\phi} e^{6(\sigma_s \log 2)^2}. \tag{16}$$

(**a**) Isometric view   (**b**) Top view   (**c**) Side view

Figure 1. 3D geometrical model of sintered metal fibre materials based on micro-CT image reconstruction. The red square plane in (**a**) denotes a slice of the micro CT scan. (**b**) Top view of the model in *x-y* plane. (**c**) Right view of the model in *x-z* plane.

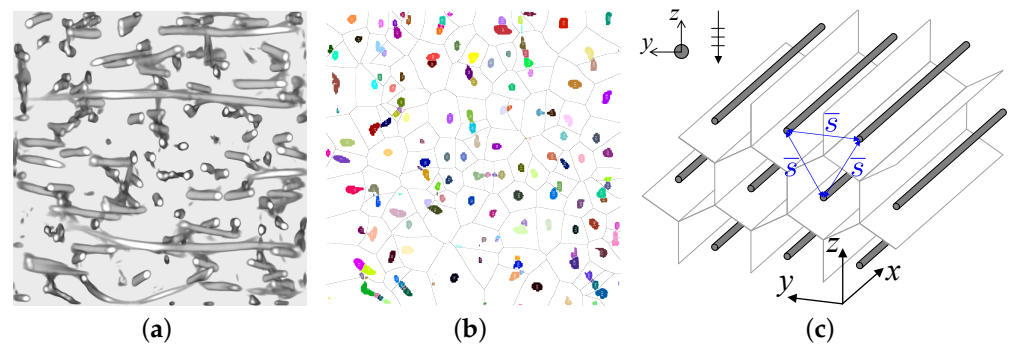**Figure 2.** (**a**) Front view of the 3D micro CT slice image at the position shown in the isometric view of the 3D model. (**b**) Voronoi diagram of the 2D slice image. (**c**) Array of parallel cylindrical fibres with ideal hexagonal Voronoi regions.

3. Measurement Configuration

The impedance tube is an acoustic measurement system for determining the sound absorption coefficient, the sound reflection coefficient, and the surface impedance of materials in the laboratory on the basis of the transfer function method according to ISO 10534-2 Standard [41].

For testing the surface impedance of our prepared fibrous metal felt samples, a custom-built impedance tube with a 50 mm × 50 mm square cross-section is designed. The data-acquisition module (m+p VibPilot) system includes two microphones (G.R.A.S. 46BD) inserted into a hole in the tube. As shown in Figure 3a, s is the distance between the microphones, and l is the distance between the surface of the felt being tested and the nearest microphone, which are equal to 50 mm. The measurements are made in the frequency range of 200 Hz to 3150 Hz.
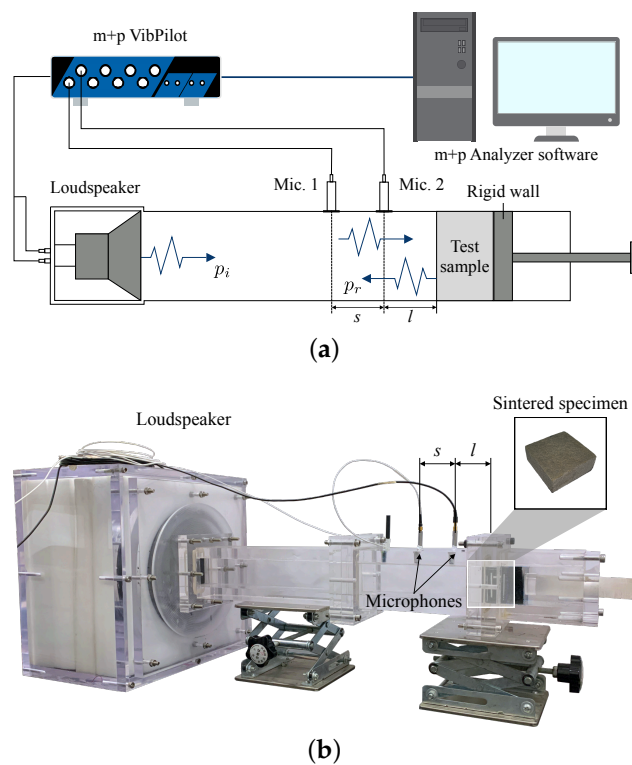

Figure 3. Acoustic measurement system used for measuring the normalised surface impedance of the prepared sintered specimens. (**a**) Schematic of the classic two-microphone impedance tube. (**b**) Realistic facility used in our test.

Overall, the sound pressure in the tube produced by the loudspeaker is measured by the microphones, and the sound reflection coefficient R is calculated via the transfer function method. Based on the obtained reflection coefficient R, the sound absorption coefficient α and surface impedance Z_s can be calculated as [22]:

$$\alpha = 1 - |R|^2, \tag{17}$$

$$Z_s = \frac{1+R}{1-R} Z_0. \tag{18}$$

where $Z_0 = \rho_0 c_0$ is the impedance of air.

With the rigid frame assumption, the characteristic impedance Z_c and the complex wave number k_c are the fundamental acoustic properties of the rigid backing fibrous materials that can completely characterise their acoustical behaviour. In this case, the measured surface impedance Z_s can also be expressed by Z_c and k_c as [22]:

$$Z_s = -jZ_c \cot(k_c t), \tag{19}$$

where t is the test sample thickness corresponding to the measured surface impedance Z_s.

4. Inverse Characterisation

4.1. Observation Model

The observational model is an error model representing the additive random noise and the uncertainty of the measurements using the impedance tube. In general, the experimental observational model can be described as:

$$y = h(\theta, \xi) + \epsilon, \tag{20}$$

where $y = [Z_s^{meas}]$ or $[Z_c^{meas}, k_c^{meas}]$ corresponding to the measurement procedures, $h(\theta, \xi)$ is the modified three-parameter model based on the JCAL model derived in Section 2, θ is a set of unknown transport parameters $[\phi, d, \sigma_s]$, ξ consists of the known environmental conditions (e.g., specific heat ratio γ, quiescent pressure P_0) and the measured thickness of felt samples t, and ϵ is the unknown factor may result from media inhomogeneity, measurement error and so on. Here, we consider the white Gaussian noise from the electric signal as the only source of the unknown factor ϵ.

4.2. Heuristic Approaches

For the purpose of estimating θ from a given y, two representative heuristic algorithms are performed. Based on the number of unknown transport parameters, inverse problems can be grouped into two categories: single-parameter and multi-parameter inversion.

In general, the porosity ϕ and fibre diameter d are the given parameters for one sintered metal fibre felt. For our modified three-parameter model, this means that only one parameter is unknown, which is the standard deviation in the pore size σ_s. Therefore, the minimisation problem reduces to a single parameter estimation, which can be solved by a local optimisation algorithm.

As a non-gradient method, the Nelder—Mead Method has been successfully implemented in some similar nonlinear optimisation schemes [42]. Here, the standard deviation σ_s is recovered from the surface impedance Z_s. The objective function is formed as:

$$\min_\theta F(\omega; \theta) = \min_\theta \left[\frac{1}{N_f} \sum_{f=f_l}^{f_u} \| Z_s^{meas}(\omega) - Z_s^{model}(\omega; \sigma_s) \| \right] \tag{21}$$

where ω is the angular frequency, N_f is the number of frequency points, f_l is the lower frequency, and f_u is the upper frequency.

During the inversion, the frequency range $f \in [500, 2500]$ at intervals of 50 Hz, the standard deviation $\sigma_s \in [0, 1]$, the starting point is set to 0.5, and the maximum number of iterations is set to 500.

In the case of totally unknown parameters of one fibrous metal sample, a global optimisation algorithm for inversion is proposed. The genetic algorithm (GA) is a non-gradient method inspired by the process of natural selection, which is the class of evolutionary algorithms [43]. Unlike the Nelder—Mead simplex algorithm, which can only find a local optimum close to the starting point, however, GA is capable of finding generally good global solutions, and no starting point is required, which makes GA easier to implement.

In this case, to study the effect of the choice of initial acoustical properties for inversion, $[\phi, d, \sigma_s]$ are recovered from the surface impedance $[Z_s^{meas}]$ and the fundamental acoustic properties $[Z_c^{meas}, k_c^{meas}]$, respectively.

The flow of GA is illustrated in Figure 4. Three transport parameters $[\phi, d, \sigma_s]$ (summarised in Table 1) are encoded as chromosomes and optimised by GA. The GA optimisation process starts from a population of individuals randomly generated in constraints, which is called initialisation. The next step is to generate another two generation populations of solutions through crossover and mutation, respectively. The crossover probability is basically set to 0.95, and the mutation probability is 0.1 for two inversion problems. To avoid producing a solution that is not physically reasonable, constraints are also employed in the process of crossover and mutation. A portion of the existing population is selected by rating the fitness of each solution to breed the next generation. Elitist selection is introduced here to guarantee that the solution quality will not decrease from one generation to the next [44]. The fitness function for recovering $[\phi, d, \sigma_s]$ from $[Z_s^{meas}]$ is analogous to Equation (21), which can be given by

$$\min_{\theta} F(\omega; \theta) = \min_{\theta} \left[\frac{1}{N_f} \sum_{f=f_l}^{f_u} \left\| \frac{Z_s^{meas}(\omega) - Z_s^{model}(\omega; \sigma_s)}{Z_s^{meas}(\omega)} \right\| \right] \tag{22}$$

for inversion from $[Z_c^{meas}, k_c^{meas}]$, the fitness function can be written as:

$$\min_{\theta} F(\omega; \theta) = \min_{\theta} \left[\frac{1}{N_f} \sum_{f=f_l}^{f_u} \left(\left\| \frac{Z_c^{meas}(\omega) - Z_c^{model}(\omega; \phi, d, \sigma_s)}{Z_c^{meas}(\omega)} \right\| \right. \right.$$
$$\left. \left. + \left\| \frac{k_c^{meas}(\omega) - k_c^{model}(\omega; \phi, d, \sigma_s)}{k_c^{meas}(\omega)} \right\| \right) \right] \tag{23}$$

Considering the characteristic impedance and the complex wave number may have different contributions to the fitness function, the fitness function is formed as a sum of the error percentage of Z_c and k_c to make sure two complex properties can be minimised simultaneously and equally.
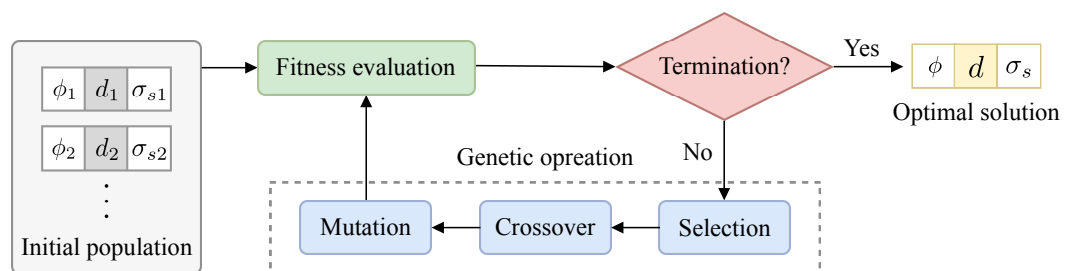

Figure 4. Outline of the genetic algorithm.

Table 1. Range values of the transport parameters set in GA.

ϕ	d (μm)	σ_s
$(0.5, 1)$	$(5, 105)$	$(0.1, 0.6)$

To increase the chance of searching the global minimum, the initial population size and the maximum number of iterations are both set to 200, and each inversion procedure will run several times due to the initial population of GA being randomly generated.

5. Results and Discussion

5.1. Theoretical Model Verification

The proposed theoretical model for sintered metal fibre materials presented in Section 2 has been validated with a set of independent experiment data. Six fibrous metal samples with 50 mm × 50 mm square cross-section are used to test the sound absorption property using the acoustic measurement system performed in Section 3. The porosity ϕ and fibre diameter d of each sintered specimen are listed in Table 2. The thickness is averaged from five sample points located around and in the centre of the specimen by using a spiral micrometer. These six sintered specimens, generally, can be grouped into two categories: samples 1–3 with gradient porosity and sample 4–6 with gradient thickness. Furthermore, the only variable between samples 2 and 5 is the fibre diameter if the slight difference in thickness is neglected. Note that samples 4–6 are cut from one complete fibrous metal material.

Table 2. Physical parameters of six sintered metal fibre materials.

Sample Number	ϕ (%)	d (μm)	Thickness (mm)
1	95	22	17.77
2	90	22	19.26
3	85	22	19.52
4	90	40	29.54
5	90	40	19.86
6	90	40	9.89

Based on the prior assumption of the log-normal distribution of pore size, the standard deviation in the pore size σ_s is the only unknown parameter that is difficult to measure directly. For this sake, the Nelder—Mead simplex algorithm stated in Section 4.2 is performed to fit the measured surface impedance Z_s curves of six felt samples. The fitting of experimental measurements by minimising the objective function (Equation (21)) is illustrated in Figure 5. Following the inverse characterisation results of six felt samples, it can be seen that the real and imaginary parts of the measured Z_s are generally fitted well by the algorithm using the theoretical model. The optimal parameter σ_s recovered from the inversion process for each sample is summarised in Table 3.
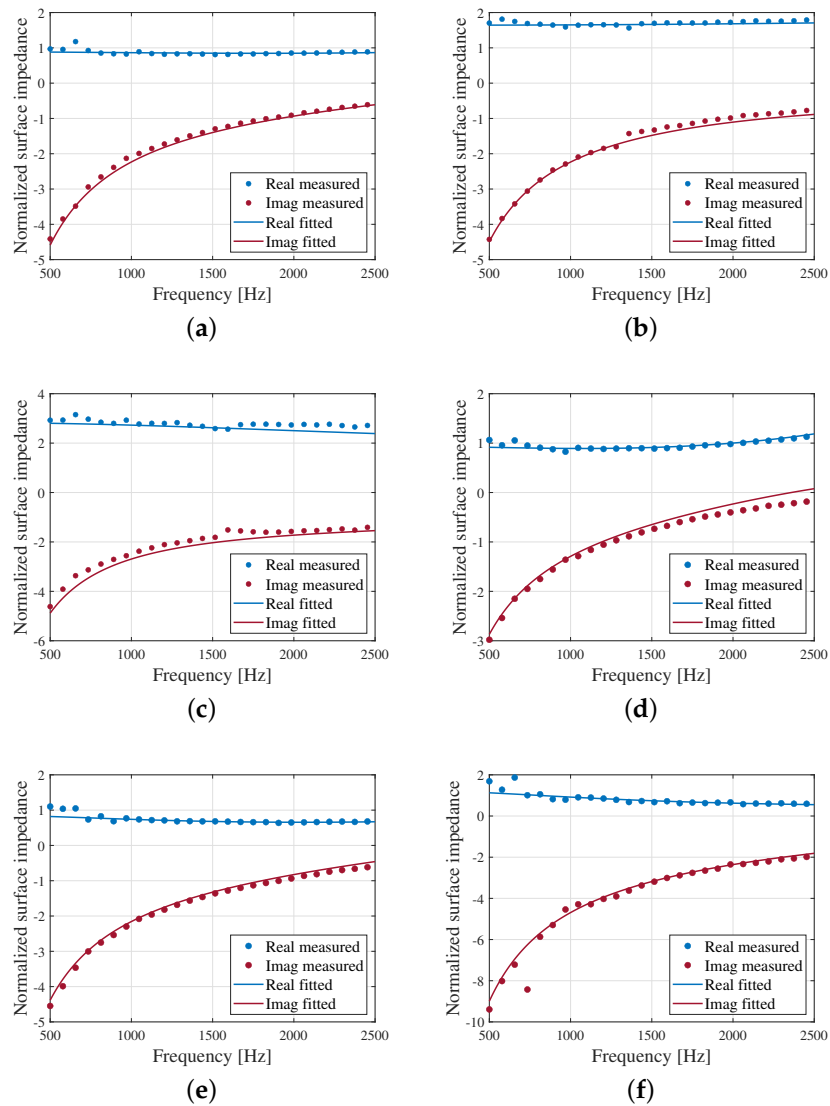
Figure 5. Fitting for the measured normalised surface impedance of six felt samples, (**a**) Sample 1, (**b**) Sample 2, (**c**) Sample 3, (**d**) Sample 4, (**e**) Sample 5, (**f**) Sample 6.

Table 3. Optimal standard deviation obtained from the inverse characterisation on the six felt samples

Sample Number	1	2	3	4	5	6
Optimal σ_s	0.4502	0.4697	0.4961	0.4486	0.4431	0.5112

　　　In order to avoid the possibility of mistaking a local minimum for a global minimum by the algorithm, the evolution of the objective function minima in the function of the standard deviation σ_s related to all samples is displayed in Figure 6. Visually, only one minimum exists in the objective function for σ_s values ranging from 0 to 1. Therefore, the transport parameter σ_s recovered from experimental Z_s by the Nelder—Mead simplex algorithm can be confirmed as a global minimum.
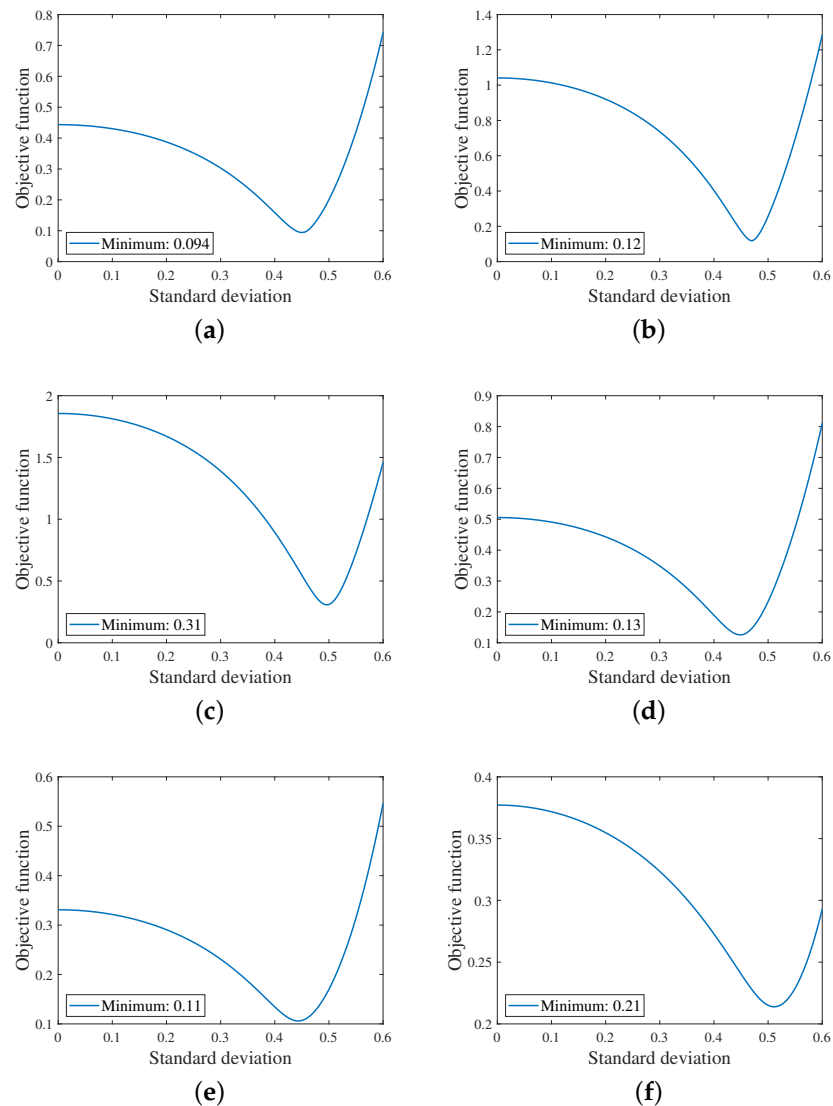
Figure 6. Minimum of the objective function for six inversion processes, (**a**) Sample 1, (**b**) Sample 2, (**c**) Sample 3, (**d**) Sample 4, (**e**) Sample 5, (**f**) Sample 6.

As previously derived in the theoretical model, the five of six transport parameters in the JCAL model can be expressed via three pore parameters, using Equations (12)–(16). The complete set of non-acoustical parameters in the JCAL model for these samples, calculated by two known physical parameters $[\phi, d]$ and the identified parameter σ_s based on the modified three-parameter model, are summarised in Table 4. The estimated values of five parameters seem sensible in their ranges, respectively, compared with those of fibrous felts reported in other literature. By comparing the transport parameters of each sintered felt sample in Tables 3 and 4, the standard deviation σ_s of samples 1–3 increases gradually with the decrease in the porosity. For the comparison between samples 2 and 5, fibre diameter d is inversely proportional to the standard deviation σ_s. As for samples 4–6, a good coincidence between samples 4 and 5 is observed, while sample 6 has apparent discrepancies with non-acoustical parameters in the other two samples. This may attribute to inhomogeneity across the complete sintered metal fibre materials incurred by manufacturing defects. In summary, the value of standard deviation σ_s range from 0.4 to 0.5 and be insensitive to the changes of the other two parameters. It is noted that the tortuosity of a fibrous metal (defined in Equation (7)) with the log-normal distributed pore size depends only on the standard deviation σ_s.

Table 4. Results of the non-acoustical parameters in the JCAL model for six felt samples.

Sample Number	ϕ	σ (N·s·m^{-4})	α_{∞}	Λ (µm)	Λ' (µm)	k_0' (µm^2)
1	0.95	41,954.06	1.48	77.13	113.86	13041.30
2	0.90	96,559.47	1.53	53.37	81.56	27060.14
3	0.85	173,335.58	1.60	42.27	67.83	41938.14
4	0.90	26,613.63	1.47	99.33	146.24	8339.47
5	0.90	25,989.77	1.46	99.92	145.72	8379.13
6	0.90	35,521.69	1.65	92.41	152.71	7871.56

Moreover, a forward evaluation for the sound absorption coefficient using the JCAL model, which is calculated by six non-acoustical parameter $[\phi, \sigma, \alpha_{\infty}, \Lambda, \Lambda', k_0']$ listed in Table 4, are compared with the measured data, as shown in Figure 7. The predicted sound absorption coefficient matches well with the measured curve for each felt sample.
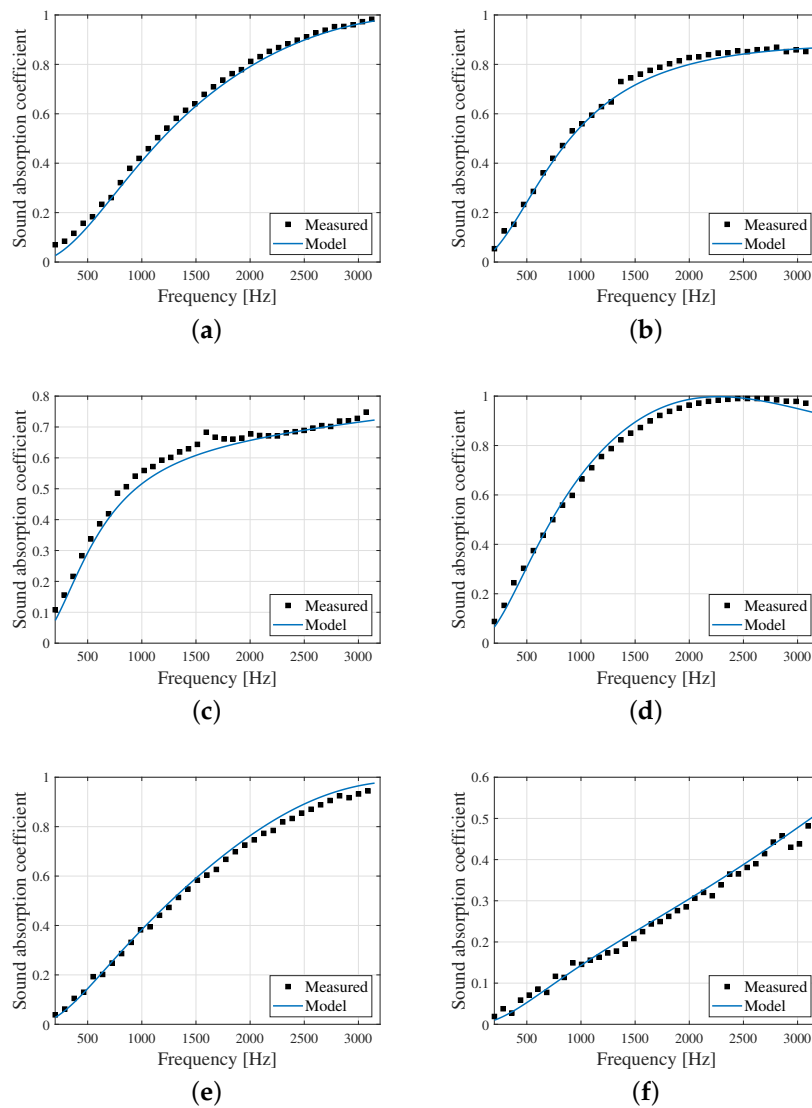

Figure 7. Comparison of the measured sound absorption coefficient and theoretical one calculated by six non-acoustical parameters based on the JCAL model for six sintered felt samples, (**a**) Sample 1, (**b**) Sample 2, (**c**) Sample 3, (**d**) Sample 4, (**e**) Sample 5, (**f**) Sample 6.

Since the fit and predicted curves are both in good agreement with the measured normalised surface impedance and sound absorption coefficient, respectively, the prior assumption on the log-normal distribution of pore size in these fibrous metal felts is verified. Overall, results have shown that our modified three-parameter theoretical model is capable of yielding accurate results for the sintered metal fibre materials.

5.2. Numerical Investigation

In a further analysis, the theoretical acoustical data generated from the established modified model is used to study the difference between two inverse problems: recovering the transport parameters from surface impedance Z_s and two porous material properties $[Z_c, k_c]$, respectively. According to the Equations (8), (9) and (19), surface impedance Z_s can be expressed by two porous material properties $[Z_c, k_c]$ with the known material thickness. For the purpose of analysing the complexity of two inverse problems, numerical parameters are adopted. In order to take both generality and particularity into consideration, three instead of one set of randomly generated transport parameters (listed in Table 5) and the corresponding acoustical data are selected. The GA presented in Section 4.2 is applied for characterising these three generated samples owing to its power for multi-parameter identification.

Table 5. Randomly generated physical parameters of fibrous metal felts for numerical investigation.

Generated Sample	ϕ	d (μm)	σ_s	Thickness (mm)
A	0.9074	95.5792	0.1635	46.1019
B	0.6535	57.4824	0.4076	34.5052
C	0.6977	15.0724	0.2074	35.1952

Due to the nature of the non-deterministic algorithm, the GA is continuously run three times with the initial population that is randomly generated within the range values in Table 1. The optimal parameters obtained in each run for two inverse problems are summarised in Table 6, and the relative errors between the theoretical and optimal parameters are given together for intuitive understanding. The best fitness values of each run are also provided as a reference. The iterative process of GA takes approximately 2.8 s on a Intel® Core™ i7-9700 processor for each run.

As shown in Table 6, the same transport parameter obtained in any two trials for the same input parameters differs from each other. Meanwhile, the variation trend of the error relative to the theoretical value is also irregular. Actually, as a typical population-based global search meta-heuristic, the GA is capable of identifying near-optimal solutions among the local optimums but cannot guarantee that a global optimal solution can be found. In comparison, local search-based strategies such as the Newton—Raphson Method and Nelder—Mead simplex algorithm (presented in Section 4.2) are dependent on initial guesses and easily plunge into the local optimum. This is an important factor in the choice of GA to compare the complexity of two inverse problems.

Table 6. Transport parameters identified using GA from the surface impedance Z_s and two acoustic properties $[Z_c, k_c]$ with relative errors between the theoretical and optimal values. The mean relative errors for each input parameter are given in boldface.

Generated Sample	Input Parameters	Number	$\phi \pm$ Error (%)	d (μm) $\pm$ Error (%)	$\sigma_s \pm$ Error (%)	Fitness Value
A	Z_s	#1	0.9156 (+0.91)	90.9148 (−4.88)	0.1654 (+1.14)	0.0074
		#2	0.9123 (+0.55)	92.8670 (−2.84)	0.1653 (+1.11)	0.0045
		#3	0.9241 (+1.84)	86.2075 (−9.81)	0.1692 (+3.50)	0.0151
		Mean	**0.9173 (+1.09)**	**89.9964 (−5.84)**	**0.1666 (+1.90)**	
	$[Z_c, k_c]$	#1	0.9074 (+0.001)	95.6981 (+0.12)	0.1640 (+0.28)	3.2359×10^{-4}
		#2	0.9113 (+0.43)	94.3968 (−1.24)	0.1761 (+7.69)	0.0035
		#3	0.9166 (+1.02)	92.5786 (−3.14)	0.1912 (+16.93)	0.0083
		Mean	**0.9118 (+0.48)**	**94.2245 (−1.42)**	**0.1771 (+8.32)**	
B	Z_s	#1	0.6344 (−2.93)	60.2355 (+4.79)	0.4067 (−0.22)	0.0149
		#2	0.6960 (+6.50)	54.7718 (−4.72)	0.4350 (+6.73)	0.0233
		#3	0.6492 (−0.66)	63.8648 (+11.10)	0.4476 (+9.83)	0.0260
		Mean	**0.6599 (+0.97)**	**59.6240 (−3.73)**	**0.4298 (+5.44)**	
	$[Z_c, k_c]$	#1	0.6545 (+0.14)	55.8480 (−2.84)	0.3934 (−3.48)	0.0120
		#2	0.6508 (−0.41)	55.5301 (−3.40)	0.3875 (−4.93)	0.0130
		#3	0.6483 (−0.80)	56.9729 (−0.89)	0.3963 (−2.77)	0.0065
		Mean	**0.6512 (−0.35)**	**56.1170 (−2.38)**	**0.3924 (−3.73)**	
C	Z_s	#1	0.8859 (+26.97)	13.4143 (−11.00)	0.5449 (+162.71)	0.0117
		#2	0.8081 (+15.83)	15.8471 (+5.14)	0.4688 (+126.00)	0.0089
		#3	0.7293 (+4.53)	15.2246 (+1.01)	0.2976 (+43.48)	0.0020
		Mean	**0.8078 (+15.78)**	**14.8287 (−1.62)**	**0.4371 (+110.75)**	
	$[Z_c, k_c]$	#1	0.7048 (+1.02)	19.0428 (+26.34)	0.3826 (+84.43)	0.0162
		#2	0.7031 (+0.77)	16.1080 (+6.87)	0.2747 (+32.41)	0.0084
		#3	0.7012 (+0.50)	13.9150 (−7.68)	0.1122 (−45.92)	0.0064
		Mean	**0.7030 (+0.76)**	**16.3553 (+8.51)**	**0.2565 (+23.67)**	

For ease of comparison, the mean relative errors of transport parameters identified from two input parameters are illustrated in Figure 8 for three generated samples, respectively. In terms of comparing the effect of input parameters upon the inversion of transport parameters in one generated sample, inversion from $[Z_c, k_c]$ shows lower errors than the Z_s. For these two inverse problems, variations in the input parameters lead to differences in the fitness function. The best fitness value in each trial is very close to the optimal solution ($F(\omega; \theta) = 0$) while always being unequal at our limited attempts, which means the fitness functions may have multiple near-optimal solutions that are sufficiently close to the optimum. The optimisation algorithm seems to be easier to get stuck at a locally optimal value in inverse characterisation from Z_s than from $[Z_c, k_c]$. The nearest optimal solution searched by the GA appeared at trial #1 in inversion from $[Z_c, k_c]$ of sample A, whose porosity with 0.001% error can be regarded as an exact value. Meanwhile, it is noted that the relative error of porosity is found to be generally lower than the other two parameters in comparing each transport parameter. Additionally, the identified results recovered from two input parameters of sample C are visibly inferior to the other two samples, especially for the standard deviation σ_s.
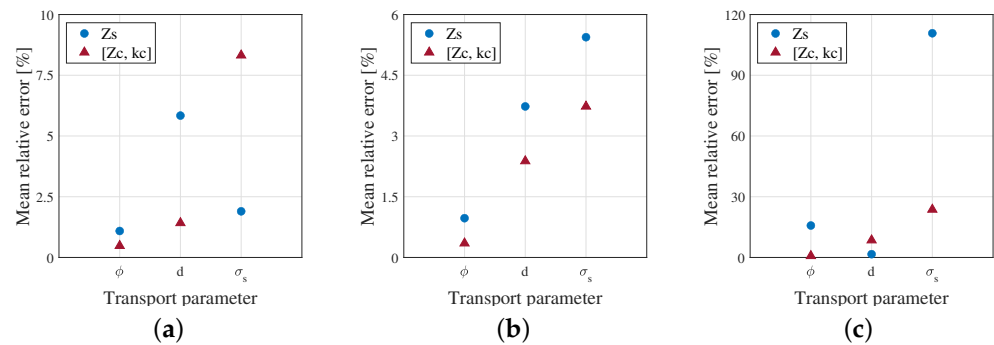
Figure 8. Comparison of the mean relative error of transport parameters identified from the surface impedance Z_s and two acoustic properties $[Z_c, k_c]$ for three generated samples, (**a**) Sample A, (**b**) Sample B, (**c**) Sample A.

For further investigating the causes of error in searching the global minima, sample C is selected as a typical one to examine the difference in characteristics of fitness function between using Z_s and $[Z_c, k_c]$ as input parameters to determine three transport parameters $[\phi, d, \sigma_s]$. As illustrated in Figures 9–11, the three-dimensional (3D) profiles of the fitness function are performed by fixing one of three parameters and varying the other two. Due to the fact that the objective and near-optimal solutions of functions distribute in a narrow region close to 0, which could hardly be identified on a 3D surface, the logarithmic transformation is performed for two fitness functions to amplify the differences in number and characteristics of local minimums. Moreover, a two-dimensional (2D) cross section is plotted at $Log(Fitness) = -2$, i.e., fitness value equals to 0.01. The section derived from this plane intersecting the curved surface is the so-called contour, which is plotted on the 2D projection plane of function. According to the Equations (22) and (23), fitness functions of GA are measured by the normalised mean error (NME). Thus, the 3D surface under the drawn 2D cross-section is composed of the solutions with the NME of $\pm 1\%$. Correspondingly, the local and global minimums are located in the area composed of axes and contour lines on the 2D projection plane.

Considering the mean relative error of identified porosity in sample C is significantly lower than the other two parameters, a detailed analysis is performed with a theoretical value and two fixed porosity values selected from $(0.70, 0.88)$ obtained in six trials, as shown in Figure 9. The range values of fibre diameter are also narrowed to $(5, 25)$ based on the results of six trials. It can be clearly seen that every sampling surface has at least one valley, which means there are an amount of equal and unequal local optimums for both two fitness functions. The depth of a valley measures the degree of closeness between the local and global minimum. Note that the global minima are both $F(\omega; \theta) = 0$ for two inversion problems, which means the logarithm of global minima actually goes to negative infinity as sampling space increases. A combination of prominence and the number of valleys directly leads to the difficulty in achieving global optimisation. The lots of comb-like valleys in Figure 9a–c and e would lead the search algorithm to converge to a wrong optimal point and hard to jump from the local optimal position. Conversely, global optimisation techniques could generally avoid the smooth valleys displayed in Figure 9d,f.
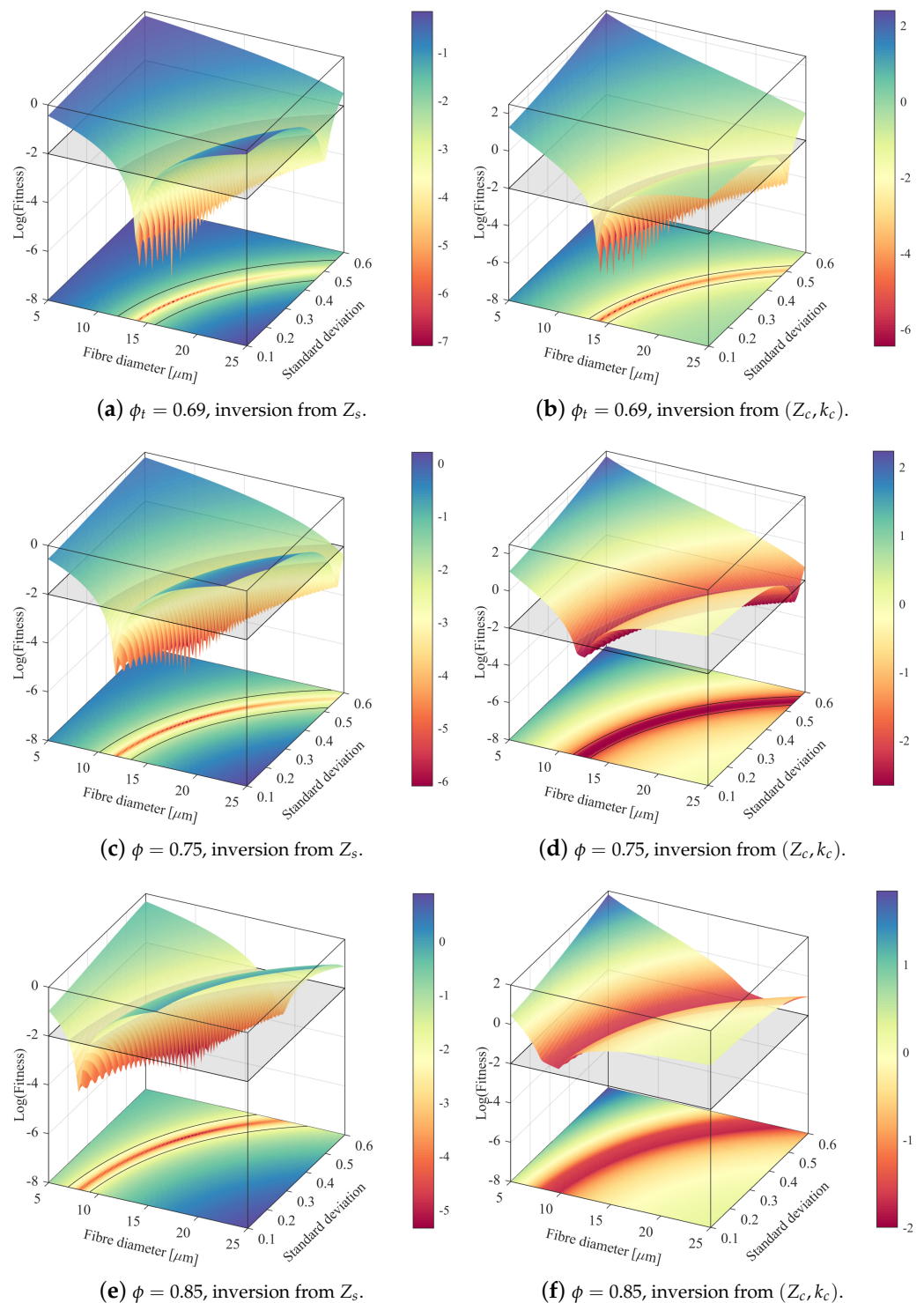
(**a**) $\phi_t = 0.69$, inversion from Z_s.

(**b**) $\phi_t = 0.69$, inversion from (Z_c, k_c).

(**c**) $\phi = 0.75$, inversion from Z_s.

(**d**) $\phi = 0.75$, inversion from (Z_c, k_c).

(**e**) $\phi = 0.85$, inversion from Z_s.

(**f**) $\phi = 0.85$, inversion from (Z_c, k_c).

Figure 9. 3D profile of the logarithm of fitness function versus the fibre diameter d and standard deviation σ_s with the fixed porosity ϕ, and 2D projection along $d - \sigma_s$ plane with contour plot at $Log(Fitness) = -2$. (**a,c,e**) Varying different porosity to investigate inverse characterisation from the surface impedance Z_s. (**b,d,f**) Varying different porosity to investigate inverse characterisation from two porous material properties $[Z_c, k_c]$.
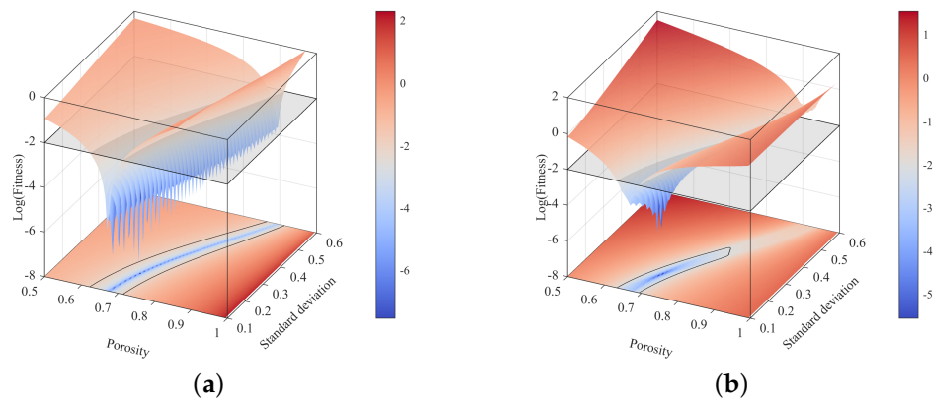
Figure 10. 3D profile of the logarithm of fitness function versus the porosity ϕ and standard deviation σ_s with the fixed fibre diameter d, and 2D projection along $\phi - \sigma_s$ plane with contour plot at $Log(Fitness) = -2$, (**a**) $d_t = 15.07$, inversion from Z_s, (**b**) $d_t = 15.07$, inversion from (Z_c, k_c).
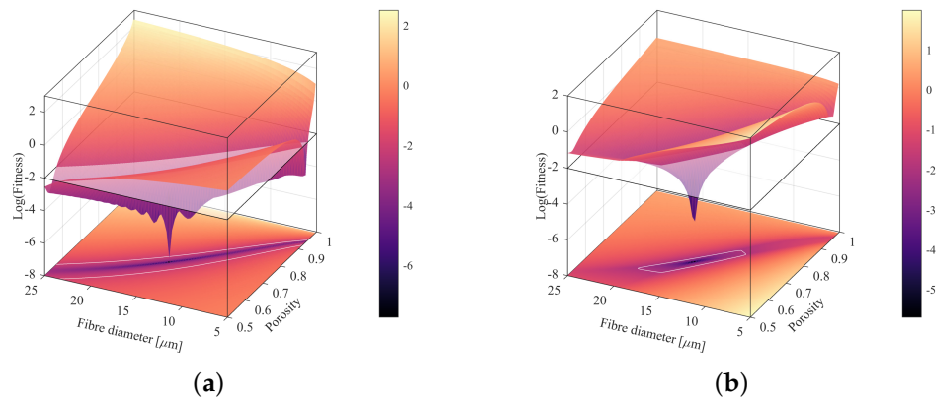

Figure 11. 3D profile of the logarithm of fitness function versus the porosity ϕ and fibre diameter d with the fixed standard deviation σ_s, and 2D projection along $\phi - d$ plane with contour plot at $Log(Fitness) = -2$, (**a**) $\sigma_s^t = 0.21$, inversion from Z_s, (**b**) $\sigma_s^t = 0.21$, inversion from (Z_c, k_c).

Visually, fitness function using Z_s as input parameters shows a complex search space which has numerous minimum "traps" in Figure 9c,e, while function with $[Z_c, k_c]$ shows a relatively smooth search space with fewer minimum "traps" in Figure 9d,f. This explains the reason why the relative errors of the identified porosity recovered from Z_s are apparently higher than those from $[Z_c, k_c]$ in general, even though part of the identified parameters inversion from Z_s is a little better than those from $[Z_c, k_c]$.

The surfaces presented in Figure 9a,b show the common feature that both have lots of comb-like valleys. In other words, there are multiple sets of near-optimal solutions $[d, \sigma_s]$ around the theoretical value of porosity, which interprets the cause of significant errors in the fibre diameter d and standard deviation σ_s recovered from both two inversion problem.

Further, another two 3D profiles of the fitness function are also provided by letting d and σ_s to be constant, respectively, as shown in Figures 10 and 11. In comparison of (a) and (b) in these two figures, overall, the valleys in the fitness function using $[Z_c, k_c]$ as input parameters have fewer numbers and more concentrated distribution than those in the function with Z_s. Especially, only one minimum, i.e., optimal solution, can be found in Figure 11b. This in turn explains the intrinsic cause of the larger error in searching the standard deviation. Overall, one can conclude from the comparison of Figures 9–11 horizontally that the fixing of one value in $[d, \sigma_s]$ can largely improve the optimisation quality and efficiency, or the difficulty in determining fibre diameter and standard deviation from Z_s or $[Z_c, k_c]$ is obviously higher than in determining porosity. Actually, global optimisation

of the fitness function is processed on all three parameters simultaneously, which means the search space is far more complicated than the 3D surface shown in Figures 9–11. The combination of these factors results in the complexity of inverse characterisation from acoustical data and deviations of objective variables to a different degree. In general, the multiple execution results of GA and the detailed investigation of sample C for two inverse problems both indicate that inversion from two porous material properties $[Z_c, k_c]$ is preferable to surface impedance Z_s.

6. Conclusions

In this study, two heuristic approaches are, respectively, performed to validate the proposed modified three-parameter model by impedance tube measurement and investigate the effects of two input acoustical parameters on the inverse characterisation of sintered metal fibre materials. A new set of transport parameters in the modified three-parameter model based on the JCAL model for the acoustical properties of porous media is provided. A satisfactory result is achieved in fitting the normalised surface impedance measured by an acoustic measurement system for six sintered specimens with varying porosity, fibre diameter, and thickness. With the established modified model, a numerical investigation is performed to study the difference between recovering all three transport parameters from surface impedance and from two porous material properties. The several execution results of GA and further analysis of two fitness functions indicate that the search space in inversion from surface impedance is more complex than that from the characteristic impedance and the complex wave number.

Differing from the previous works on direct, indirect, or inverse methods based on the five or six-parameter acoustical model, our modified three-parameter model and inverse characterisation method realise effective and accurate inverse acoustic characterisation of sintered metal fibre materials. The accuracy of our modified three-parameter theoretical model is validated by experiments. Based on the proposed modified three-parameter model, the sintered metal fibre materials with two known customised microstructure parameters can be accurately characterised using a local optimisation algorithm. Complete inverse acoustic characterisation of fibrous metals from the characteristic impedance and the complex wave number is proved to be more accurate than from the normalised surface impedance by a global optimisation algorithm. Our future work will concentrate on developing new methods to improve accuracy for inverse characterising various porous materials based on this modified three-parameter model.

References

1.   Lu, T.; He, D.; Chen, C.; Zhao, C.; Fang, D.; Wang, X. The multi-functionality of ultra-light porous metals and their applications. *Adv. Mech.* **2006**, *36*, 517–535.
2.   Huiping, T.; Jianzhong, W.; Qingbo, A.; Hao, Z. Effect of pore structure on performance of porous metal fiber materials. *Rare Met. Mater. Eng.* **2015**, *44*, 1821–1826. [CrossRef]
3.   Sun, W.; Pan, B.; Song, X.; Xiao, H.; Zhou, J.; Sui, D. A novel sound absorber design of nanofibrous composite porous material. *Mater. Des.* **2022**, *214*, 110418. [CrossRef]
4.   Sun, F.; Chen, H.; Wu, J.; Feng, K. Sound absorbing characteristics of fibrous metal materials at high temperatures. *Appl. Acoust.* **2010**, *71*, 221–235. [CrossRef]
5.   Delany, M.; Bazley, E. Acoustical properties of fibrous absorbent materials. *Appl. Acoust.* **1970**, *3*, 105–116. [CrossRef]
6.   Miki, Y. Acoustical properties of porous materials-Modifications of Delany-Bazley models. *J. Acoust. Soc. Jpn. (E)* **1990**, *11*, 19–24. [CrossRef]
7.   Johnson, D.L.; Koplik, J.; Dashen, R. Theory of dynamic permeability and tortuosity in fluid-saturated porous media. *J. Fluid Mech.* **1987**, *176*, 379–402. [CrossRef]
8.   Champoux, Y.; Allard, J.F. Dynamic tortuosity and bulk modulus in air-saturated porous media. *J. Appl. Phys.* **1991**, *70*, 1975–1979. [CrossRef]
9.   Allard, J.F.; Champoux, Y. New empirical equations for sound propagation in rigid frame fibrous materials. *J. Acoust. Soc. Am.* **1992**, *91*, 3346–3353. [CrossRef]
10. Lafarge, D.; Lemarinier, P.; Allard, J.F.; Tarnow, V. Dynamic compressibility of air in porous structures at audible frequencies. *J. Acoust. Soc. Am.* **1997**, *102*, 1995–2006. [CrossRef]
11. Pride, S.R.; Morgan, F.D.; Gangi, A.F. Drag forces of porous-medium acoustics. *Phys. Rev. B* **1993**, *47*, 4964. [CrossRef]
12. Biot, M.A. Theory of elastic waves in a fluid-saturated porous solid. 1. Low frequency range. *J. Acoust. Soc. Am.* **1956**, *28*, 168–178. [CrossRef]
13. Biot, M.A. Theory of propagation of elastic waves in a fluid-saturated porous solid. II. Higher frequency range. *J. Acoust. Soc. Am.* **1956**, *28*, 179–191. [CrossRef]
14. Yuan, T.; Song, X.; Xu, J.; Pan, B.; Sui, D.; Xiao, H.; Zhou, J. Tunable acoustic composite metasurface based porous material for broadband sound absorption. *Compos. Struct.* **2022**, 116014. [CrossRef]
15. Zarastvand, M.; Asadijafari, M.; Talebitooti, R. Improvement of the low-frequency sound insulation of the poroelastic aerospace constructions considering Pasternak elastic foundation. *Aerosp. Sci. Technol.* **2021**, *112*, 106620. [CrossRef]
16. Rahmatnezhad, K.; Zarastvand, M.; Talebitooti, R. Mechanism study and power transmission feature of acoustically stimulated and thermally loaded composite shell structures with double curvature. *Compos. Struct.* **2021**, *276*, 114557. [CrossRef]
17. Zarastvand, M.; Ghassabi, M.; Talebitooti, R. Prediction of acoustic wave transmission features of the multilayered plate constructions: A review. *J. Sandw. Struct. Mater.* **2022**, *24*, 218–293. [CrossRef]
18. Khayat, M.; Baghlani, A.; Najafgholipour, M. The propagation of uncertainty in the geometrically nonlinear responses of smart sandwich porous cylindrical shells reinforced with graphene platelets. *Compos. Struct.* **2021**, *258*, 113209. [CrossRef]
19. Khayat, M.; Baghlani, A.; Najafgholipour, M.A. The effect of uncertainty sources on the dynamic instability of CNT-reinforced porous cylindrical shells integrated with piezoelectric layers under electro-mechanical loadings. *Compos. Struct.* **2021**, *273*, 114336. [CrossRef]
20. Khayat, M.; Baghlani, A.; Dehghan, S.M.; Najafgholipour, M.A. Geometrically nonlinear dynamic analysis of functionally graded porous partially fluid-filled cylindrical shells subjected to exponential loads. *J. Vib. Control.* **2022**, *28*, 758–772. [CrossRef]
21. Horoshenkov, K.V. A review of acoustical methods for porous material characterisation. *Int. J. Acoust. Vib* **2017**, *22*, 92–103. [CrossRef]
22. Allard, J.; Atalla, N. *Propagation of Sound in Porous Media: Modelling Sound Absorbing Materials 2e*; John Wiley & Sons: Hoboken, NJ, USA, 2009.
23. Leclaire, P.; Kelders, L.; Lauriks, W.; Melon, M.; Brown, N.; Castagnede, B. Determination of the viscous and thermal characteristic lengths of plastic foams by ultrasonic measurements in helium and air. *J. Appl. Phys.* **1996**, *80*, 2009–2012. [CrossRef]
24. Leclaire, P.; Kelders, L.; Lauriks, W.; Glorieux, C.; Thoen, J. Determination of the viscous characteristic length in air-filled porous materials by ultrasonic attenuation measurements. *J. Acoust. Soc. Am.* **1996**, *99*, 1944–1948. [CrossRef]
25. Leclaire, P.; Umnova, O.; Horoshenkov, K.; Maillet, L. Porosity measurement by comparison of air volumes. *Rev. Sci. Instruments* **2003**, *74*, 1366–1370. [CrossRef]
26. Moussatov, A.; Ayrault, C.; Castagnède, B. Porous material characterization–ultrasonic method for estimation of tortuosity and characteristic length using a barometric chamber. *Ultrasonics* **2001**, *39*, 195–202. [CrossRef]
27. Panneton, R.; Olny, X. Acoustical determination of the parameters governing viscous dissipation in porous media. *J. Acoust. Soc. Am.* **2006**, *119*, 2027–2040. [CrossRef] [PubMed]
28. Olny, X.; Panneton, R. Acoustical determination of the parameters governing thermal dissipation in porous media. *J. Acoust. Soc. Am.* **2008**, *123*, 814–824. [CrossRef] [PubMed]
29. Bonfiglio, P.; Pompoli, F. Inversion problems for determining physical parameters of porous materials: Overview and comparison between different methods. *Acta Acust. United Acust.* **2013**, *99*, 341–351. [CrossRef]

30. Groby, J.P.; Ogam, E.; De Ryck, L.; Sebaa, N.; Lauriks, W. Analytical method for the ultrasonic characterization of homogeneous rigid porous materials from transmitted and reflected coefficients. *J. Acoust. Soc. Am.* **2010**, *127*, 764–772. [CrossRef]

31. Atalla, Y.; Panneton, R. Inverse Acoustical Characterization of Open Cell Porous Media Using Impedance Tube Measurements. *Can. Acoust. Acoust. Can.* **2005**, *33*.

32. Dauchez, N.; Yvars, P.A. *Inverse Method for Porous Material Characterization Using the Constraint Satisfaction Problem Approach*; Acoustics: Bengaluru, India, 2012.

33. Dossi, M.; Brennan, M.; Moesen, M.; Vandenbroeck, J.; Huo, L. An Inverse Method to Determine Acoustic Parameters of Polyurethane Foams. *Inter-Noise -Noise-Con Congr. Conf. Proc.* **2019**, *259*, 1170–1181.

34. Chazot, J.D.; Zhang, E.; Antoni, J. Acoustical and mechanical characterization of poroelastic materials using a Bayesian approach. *J. Acoust. Soc. Am.* **2012**, *131*, 4584–4595. [CrossRef]

35. Niskanen, M.; Groby, J.P.; Duclos, A.; Dazel, O.; Le Roux, J.C.; Poulain, N.; Huttunen, T.; Lähivaara, T. Deterministic and Statistical Characterization of Rigid Frame Porous Materials from Impedance Tube Measurements. *J. Acoust. Soc. Am.* **2017**, *142*, 2407–2418. [CrossRef]

36. Cuenca, J.; Göransson, P.; De Ryck, L.; Lähivaara, T. Deterministic and Statistical Methods for the Characterisation of Poroelastic Media from Multi-Observation Sound Absorption Measurements. *Mech. Syst. Signal Process.* **2022**, *163*, 108186. [CrossRef]

37. Horoshenkov, K.V.; Hurrell, A.; Groby, J.P. A Three-Parameter Analytical Model for the Acoustical Properties of Porous Media. *J. Acoust. Soc. Am.* **2019**, *145*, 2512–2517. [CrossRef]

38. Xie, H.; Deng, B.; et al. Latest advances of X-ray imaging and biomedical applications beamline at SSRF. *Nucl. Sci. Tech.* **2015**, *26*, 20102-020102.

39. Tarnow, V. Airflow resistivity of models of fibrous acoustic materials. *J. Acoust. Soc. Am.* **1996**, *100*, 3706–3713. [CrossRef]

40. Tarnow, V. Calculation of the dynamic air flow resistivity of fiber materials. *J. Acoust. Soc. Am.* **1997**, *102*, 1680–1688. [CrossRef]

41. *ISO 10534-2:1998*; Acoustics–Determination of Sound Absorption Coefficient And Impedance in Impedance Tubes—Part 2: Transfer-Function Method. Standard, International Organization for Standardization: Geneva, Switzerland, 1998.

42. Nelder, J.A.; Mead, R. A simplex method for function minimization. *Comput. J.* **1965**, *7*, 308–313. [CrossRef]

43. Holland, J.H. *Adaptation in Natural and Artificial Systems: An Introductory Analysis with Applications to Biology, Control, and Artificial Intelligence*; MIT press: Cambridge, MA, USA, 1992.

44. Baluja, S.; Caruana, R. Removing the genetics from the standard genetic algorithm. In *Machine Learning Proceedings 1995*; Elsevier: Amsterdam, The Netherlands, 1995; pp. 38–46.